THE ROLE OF CLAY CHARGE IN THE MOBILITY OF COMPENSATING CATIONS: AN APPROACH FROM MOLECULAR DYNAMICS

EL PAPEL DE LA CARGA DE LA ARCILLA EN LA MOVILIDAD DE LOS CATIONES DE COMPENSACIÓN: UNA APROXIMACIÓN DESDE LA DINÁMICA MOLECULAR

C. D. Marrero-Pérez [a], G. Rojas-Lorenzo[b], A. Lam[a†]

a) Zeolite Engineering Laboratory, Institute of Material Science and Technology (IMRE), University of Havana, Havana, CP. 10400. Cuba. krlodavid419@gmail.com, anabel@imre.uh.cu[†]
b) Instituto Superior de Tecnologías y Ciencias Aplicadas (InSTEC). Universidad de La Habana, La Habana - 10400, Cuba. german@instec.cu
† corresponding author

Recibido 5/2/2025; Aceptado 5/7/2025

The charge of clays plays an important role in the mobility of compensating cations and in swelling processes. In this work we have developed a method to generate Lithium Fluorhectorite (Li-Fh) clay models with a charge of -1.2*e* and a non-homogeneous charge distribution. This charge is closer to the experimentally reported value. We used this approach to study their interaction with water using Molecular Dynamics (MD) simulations. The MD simulations showed that the Li^+ diffusion coefficient increases by two orders of magnitude with decreasing clay charge. Population analyses and Li^+ coordination indicate a greater interaction of the cations with water molecules with decreasing clay charge, leading to a deformation in the stacking of clay layers in the 010 model. These results highlight the important influence of clay charge on cation dynamics and structural behaviour, providing insight into delamination and swelling mechanisms.

La carga de las arcillas desempeña un rol importante en la movilidad de los cationes de compensación y en los procesos de hinchamiento. En este trabajo hemos desarrollado un método para generar modelos de la arcilla Litio Fluorhectorita (Li-Fh) con carga igual a -1,2*e* y una distribución de carga no homogénea. Esta carga se aproxima más al valor reportado experimentalmente. Utilizando simulaciones de dinámica molecular (DM) hemos estudiado la interacción de la Li-Fh con agua. Las simulaciones de DM mostraron que el coeficiente de difusión del Li^+ aumenta en dos órdenes de magnitud con la disminución de la carga de la arcilla. Los análisis de población y la coordinación del Li^+ indican una mayor interacción del catión con las moléculas de agua al disminuir la carga de la arcilla, lo que conduce a una deformación en el apilamiento de las láminas en el modelo 010. Estos resultados ponen de relieve la importante influencia de la carga de la arcilla en la dinámica de los cationes y el comportamiento estructural, proporcionando una visión de los mecanismos de delaminación e hinchamiento.

Keywords: Molecular Dynamics Calculations (Cálculos de Dinámica Molecular); Diffusion in nanoscale solids (Difusión en sólidos en la nanoescala); Computer modeling; simulation (Modelación y simulación computacional).

I. INTRODUCTION

Clay materials, with their unique layered structures and inherent ion-exchange capabilities, are widespread in nature and indispensable in many technological applications [1]. The ability of clays to selectively adsorb and release ions is fundamental to a wide range of processes, including soil fertility management [2], wastewater treatment [3] and the development of advanced materials [4]. In agriculture, clays play a crucial role in retaining essential nutrients and regulating their availability to plants [5]. In environmental remediation, they are used to remove heavy metals and organic contaminants from contaminated water and soil [6]. Furthermore, the ion-exchange properties of clays are exploited in catalysis [7], drug delivery systems [8, 9] and the preparation of novel nanocomposites [10]. Consequently, a thorough understanding of the mechanisms governing ion exchange in clay materials is essential to optimise their performance in existing applications and to explore new opportunities in various scientific and technological fields. The isomorphic substitution of higher valence atoms for lower valence atoms within the clay framework creates a negative charge density that is neutralized by Group I and II cations, known as compensating cations. These compensating cations are located in the interlayer spaces and on the surface of the clay. Together with water molecules, they exhibit high mobility within the material. The interaction of these compensating cations with water molecules and the clay framework influences processes such as ion exchange and swelling. Smectite-type clays with charges between -0.2 and -0.6*e* are known to swell. However, in materials with higher charges, such as micas, the cation-clay lattice interactions prevent swelling [11]. Lithium fluorhectorite clay (Li-Fh) is a 2:1 layered silicate in which a fraction of the Mg^{2+} cations in the trioctahedral sites are replaced by Li^+ cations, resulting in a negative structural charge that is compensated by Li^+ ions in the interlayer space. Its chemical composition is $Li_x(Mg_{6-x}Li_x)F_4Si_8O_{20}$. Li-Fh can be delaminated into single layers by osmotic swelling in deionized water [11]. In previous work, we investigated the cation motion of Li-Fh clay models with a charge of -2*e* using molecular dynamics (MD) simulations [12]. However, the actual charge of this material is much lower, closer to -1.2*e* [13,14]. To evaluate the influence of clay charge on the movement of Li^+ compensating cations and their interaction with water, we created one hundred Li-Fh models with a charge of -1.2*e* by modifying models with a charge of -2*e*. Then, MD simulations were performed to evaluate the energy of the 100 models, and we selected the most stable one to build models representing the clay lattice in three different scenarios: in the center of the crystal (bulk model), on the surface created by removing the periodicity in the crystallographic b direction (010 model), and on the surface without periodicity along the c direction (001 model). Finally, the diffusion of Li^+ in the three models with charge -1.2*e* is studied and compared with that obtained for the model with charge -2*e*. The results obtained here will shed light on the role of clay charge in the mobility of compensating cations and their interaction with the clay framework and water, thus contributing to the understanding of complex processes such as swelling and ion exchange.

II. METHODOLOGY

In our previous studies, we employed a LiFh model consisting of 75 unit cells, generated by $5 \times 5 \times 3$ replication of the LiFh unit cell along the crystallographic axes [12, 15]. In each unit cell of those models, two magnesium atoms in the octahedral sheet were replaced by two lithium atoms, resulting in a -2*e* charge balanced by two lithium compensating cations (Li^+). The unit cell formula was $Li_2^+(Mg_4Li_2)F_4Si_8O_{20} \times 12H_2O$. However, this model overestimates the true charge, which is closer to -1.2*e* [13, 14]. Therefore, we developed a method to adjust the charge of the initial model [12, 15] and generate models with a -1.2*e* charge. This involved randomly replacing one lithium atom in the octahedral layer with a magnesium atom and removing one Li^+ compensating cation in 60 of the 75 unit cells, resulting in unit cells with the formula $Li^+(Mg_5Li)F_4Si_8O_{20} \times 12H_2O$. The remaining 15 unit cells retained the original formula $Li_2^+(Mg_4Li_2)F_4Si_8O_{20} \times 12H_2O$. In this way, 100 different periodic models with a non-homogeneous charge distribution of -1.2*e* were created. The Python code used in this study is available in Section S1 of the Supporting Information. The interatomic interactions in lithium fluorohectorite (LiFh) were modeled using the CLAYFF force field [16], with minor modifications to the atomic charges to ensure electroneutrality. CLAYFF incorporates electrostatic interactions, which are calculated using coulombic forces, and van der Waals interactions, which are described using a 12-6 Lennard-Jones potential. For model 010, the surface OH valence-compensating groups were modeled using Morse potential terms for edge surfaces, as proposed by Pouvreau et al [17]. However, as explained in previous work, the angle term and water potential proposed by Pouvreau et al. could not be fitted to our model [12]. We adopted the parameters of the Li^+ compensating cation, including its charge (+1*e*) and Lennard-Jones coefficients, from Koneshan et al [18]. The full details of the charges and parameters used in the CLAYFF force field can be found in Section S2 of the Supporting Information. Molecular dynamics (MD) simulations were performed using the DL_POLY code [19] to determine the total energy of the 100 periodic models. The first MD calculations were performed in the NVE ensemble during 20 ps at 300 K, with temperature control during the first 10 ps. The time step used in all simulations was 1fs. The ten models with the lowest energy were selected and additional MD simulations were performed. The second MD simulations were done in the NVE ensemble during 200 ps without temperature control. Finally, 200 ps MD runs were performed in the NPT ensemble to allow the models to adjust the volume. In all simulations the temperature was set to 300 K and the pressure in the NPT simulations was 1atm. At the end of the third MD simulation, the total energy of the ten models was evaluated and compared to select the most stable one.

The most stable model of charge -1.2*e* was used to build three different models to evaluate the Li^+ movement, see Figure 1. The first is the periodic model resembling the clay bulk. The other two models were constructed by cleaving the periodicity in the crystallographic directions b and c, as described in reference [12], and were designated 010 and 001. These two models are in contact with a water reservoir containing 1493 and 1205 water molecules, respectively, and were equilibrated as described in reference [12]. Once the three models (bulk, 010 and 001) were perfectly equilibrated, the 20 ns production runs were performed in the NPT ensemble at a pressure of 1 atm and a temperature of 300 K, with an integration time step of 1 fs. The Nosé-Hoover thermostat and barostat were used [20, 21], each with a relaxation time of 100 fs. Periodic boundary conditions were applied in all simulations, and the Ewald summation method was used to calculate the electrostatic interactions of the systems [22, 23]. The cutoff for long-range interactions -Coulomb and Lennard-Jones potentials- was set to 10 Å. The trajectory of the atoms in the NPT simulations was collected every 5000 steps for dynamics and structure analysis. Radial distribution functions (rdf), the population functions (n(r)), and the Li^+ coordination were calculated and collected every 5ps for the interaction of the Li^+ with the oxygens of clay (O_{clay}) and oxygens of water (OW). The Diffusion coefficient and the type of motion of Li^+ cations were also determined. The diffusion coefficient (D) for each elemental species was calculated from molecular dynamics (MD) trajectories using the Einstein-Smoluchowski relation, which relates D to the asymptotic slope of the mean squared displacement (MSD) in the diffusive regime [22, 23]. In DL_POLY, the atomic displacements were analyzed by calculating the MSD from particle trajectories recorded in the HISTORY file at 5000 step intervals, with ensemble averaging over all particles of each element and multiple time origins. The diffusion coefficient was determined by linear regression of the MSD(t) curve according to:

$$D = \frac{1}{6N} \lim_{t \to \infty} \frac{d}{dt} \sum_{i=1}^{N} |\vec{r}_i(t) - \vec{r}_i(0)| \quad (1)$$

where N is the number of particles for the particular element, and $\vec{r}_i(t)$ is the position vector of particle i at time t. The linear regime has been carefully identified by excluding the initial short-time ballistic motion (typically $t < 10$ ps). This methodology is well established for equilibrium systems and has been rigorously validated against both theoretical predicions and experimental measurements for comparable systems.

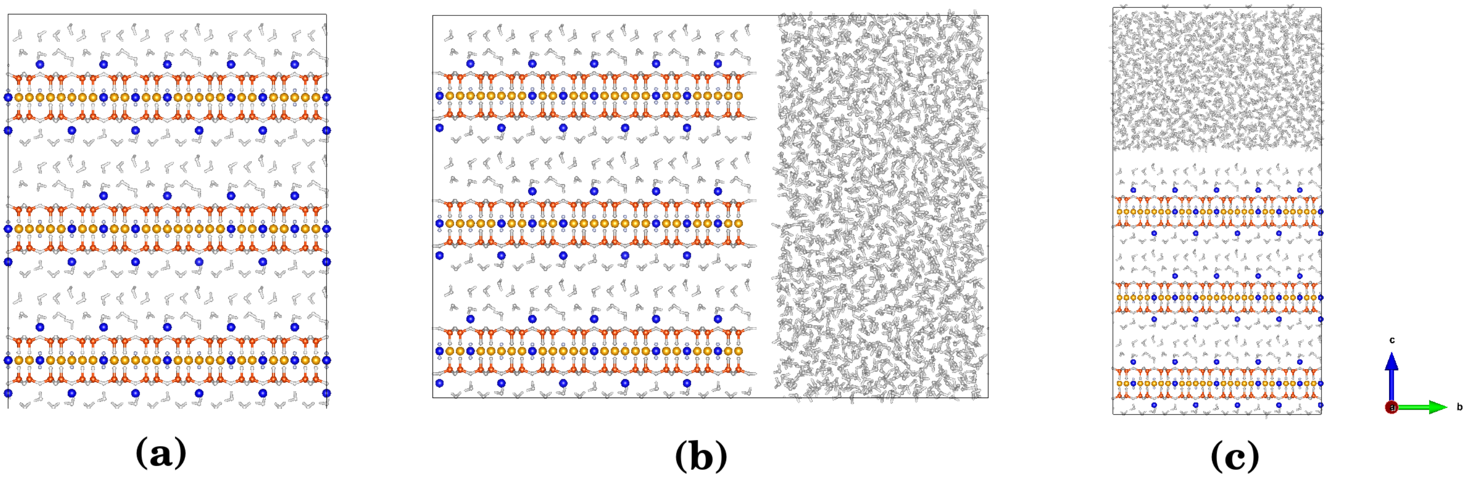
(a)

(b)

(c)

Figure 1. The models of charge -1.2e used in the simulations, (a) bulk model, (b) 010 model, (c) 001 model. The orange, gray, blue, yellow, pink, and white spheres correspond to Si, O, Li, Mg, F, and H atoms, respectively. The simulation boxes are enclosed by the black rectangles.

III. RESULTS AND CONCLUSIONS

The relative energies of the most stable models are shown in Table 1. They have been calculated as the energy difference with the model of lower energy. Model 31 exhibits the highest stability, with an energy difference of 40 kcal/mol compared to the other models. The thermal energy of the system is negligible compared to this energy gap (see Section S3 of the Supporting Information for details).

Table 1. Relative energies of the ten most stable models.

Models	ΔE (kcal/mol)
31	0
7	40
53	60
15	60
75	70
65	70
36	70
21	70
62	80

Therefore, thermal fluctuations cannot explain the observed differences in stability between the models. In model 31, the unit cells with $q = -2e$, which we consider defects, are distributed among the three clay layers: six in one layer and four or five in the other two layers. Model 31 was then used to create three clay models: bulk, 010, and 001 (see Figure 1).

As in our previous work related to the movement of Li$^+$ in the $-2e$ charged LiFh model [12], we want to evaluate the Li$^+$ diffusion in different environments represented by our three models and relate this diffusion to the clay charge. In the models with $-1.2e$ charge, we observed a significant number of Li$^+$ cations moving from their initial positions located near the hexagonal cages inside the clay layer. Of the 90 Li$^+$ ions in each model, 84 moved from their initial positions in the bulk model, while 80 and 78 moved in the 010 and 001 models, respectively.These results contrast sharply with our previous results for the $-2e$ charged model, where only 20 of 150 Li$^+$ cations moved from their initial positions in the 010 model [12].

This comparison highlights the critical role of clay charge in influencing the mobility of compensating cations, which has implications for all related properties and applications of this material. During the 20 ns simulations, Li$^+$ cations exhibited several types of motions: (I) remaining in their initial position, (II) moving to another hexagonal cage within the same layer, (III) moving to the interlayer space, (IV) diffusing into the outer water reservoir (for 010 and 001 models), (V) crossing the interlayer and occupying the opposite layer, (VI) diffusing to another layer, and (VII) moving to an octahedral edge. Movements VI and VII were only observed in the 010 model after movements III and IV. Figure 2 shows a schematic representation of these motions in the 010 model.

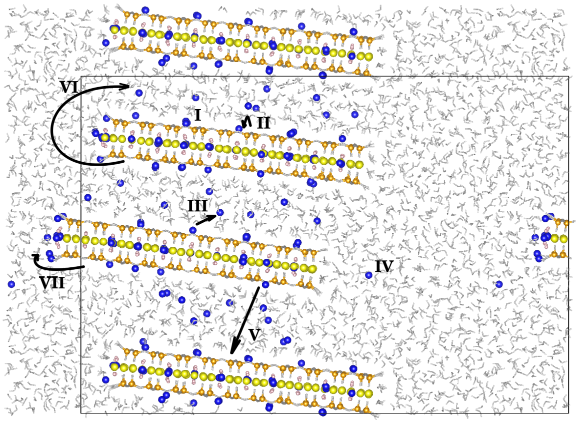

Figure 2. Schematic representation of the possible Li$^+$ motions at the 2 ns of 010 simulation. Various movements of the Li$^+$ cations in the 010 model are depicted and denoted using Roman numerals as explained in the text. The simulation box is indicated within the black rectangle, and boundary conditions were applied to enhance visualization. The orange, grey, blue, yellow, pink and white spheres correspond to Si, O, Li, Mg, F and H atoms respectively.

Table 2 shows the number of Li^+ cations that remained in their initial positions (I) and those that diffused via different types of motion. As shown, only six Li^+ ions remained in their initial positions in the bulk model, compared to 10 and 12 in the 010 and 001 models, respectively. This suggests a stronger interaction between the clay and its native cations at the edges.

Table 2. Li cations moving in the three models organized by the type of movement. (I) remaining in their initial position, (II) moving to another hexagonal cage within the same layer, (III) moving to the interlayer space, (IV) diffusing into the outer water reservoir (for 010 and 001 models), (V) crossing the interlayer and occupying the opposite layer, (VI) diffusing to another layer, and (VII) moving to an octahedral edge.

Type of movement of Li^+	**Bulk**	**010**	**001**
I	6	10	12
II	24	23	17
III	37	18	29
IV	-	18	14
V	23	12	18
VI	-	15	-
VII	-	12	-

In the bulk model, 24 Li^+ cations moved to another hexagonal cage within the same layer, 37 diffused into the interlayer region, and 23 crossed the interlayer and occupied positions in the opposite layer. In the 001 model, 17 Li^+ ions moved to another hexagonal cage within the same layer, 18 diffused into the opposite layer, and 29 were located in the interlayer region. During the simulation, 19 of 30 Li^+ ions diffused into the outer water reservoir. At the end of the simulation, 14 cations remained in the outer water reservoir and 5 cations had diffused beyond the 30 Å width of the water reservoir and settled in the opposite layer. In contrast, in the 001 model with a -2*e* charge, only 2 Li^+ cations diffused into the water reservoir during simulation [12]. This further emphasizes the strong relationship between the clay charge and the mobility of the compensating cations.

Clay materials, especially hectorite clays, swell when they interact with water. The amount of water in the interlayer space modulates the interactions between the clay lamellae. The cation-cation and cation-clay interactions are also modulated. Typically, clays with up to 25 weight percent water are in the crystalline swelling regime [24]. In the 010 model, the clay interacts with 2393 water molecules (900 in the interlayer space and 1493 in the external reservoir). The water content in the system is approximately 43 % by weight. This places the system in the osmotic swelling regime, suggesting that delamination of the material might be expected. The osmotic delamination of Li^+-fluorhectorite clays is known to result in nanolayers as thin as 1 nm (10) [11]. In water, the individual layers can arrange themselves into a "house of cards"structure, as observed at the end of the simulation in model 010. During simulation, we observed the displacement of the clay layers as they interacted with the water, including a deformation of the intermediate layer, which has the lowest charge density (see Figure SI1 and the link of the video_010 in the supporting information). This deformation results in a final system configuration that is highly deformed compared to the initial model. Figure SI2 shows the 010 reflection of the diffraction patterns of the initial configuration and the selected configurations: 0.65, 3.29, 4.05 and 5.31 ns. As can be seen, the 2θ values decrease during the simulation due to the increase in the b crystallographic parameter (from 81.94 to 83.61 Å) caused by the displacement of the clay layers. The intensity of the peaks also decreases, indicating a loss of crystallinity of the model.

Therefore, the Li^+ cation diffusion process in the 010 model undergoes motions different from those described for the bulk and 001 models. In particular, as the lamellar order is lost, a large number of cations are trapped in a space between the clay layers (about 33 Å) that contains a significant number of water molecules. This confinement of cations in such a disordered system could explain why the diffusion coefficient of Li^+ cations is lower in the 010 model than in the 001 model, as shown in Table III.

Table 3. Diffusion coefficients (D) of the Li^+ and water molecules in the clay models.

Model charge	**D** ($\times 10^{-9}$ m^2 s^{-1})				
	q = -1.2e			**q = -2e**^{a}	
Model	**Bulk**	**010**	**001**	**010**	**001**
Li^+	0.1581	0.1876	0.3171	1.2427×10^{-3}	6.3917×10^{-3}
OW	1.8022	3.9434	2.7717	4.1367	3.0629

[a] Reference [12]

The diffusion coefficients (D) of the LiFh models with charge -1.2*e* are two orders of magnitude higher than those of the models with charge of -2*e* (Table 3), consistent with our previous discussion indicating that Li^+ mobility is greater in lower charged clay models. Table 3 also shows that in the LiFh models with q=-1.2*e*, the diffusion coefficients are very similar, following the trend 001 > 010 > Bulk. As discussed above, the lower D value observed in the 010 model compared to the 001 model is attributed to the confinement of Li^+ cations in the deformed interlayer region. The lower D value of the bulk model can be associated with the greater confinement of Li^+ cations within the interlayer, which restricts their movement compared to the models with surfaces in contact with a water reservoir. This confinement effect in the bulk model is also responsible for the lower D value of the water molecules.

To further characterize the diffusion mechanism, we analyzed the mean square displacement (MSD) of Li^+ cations versus time (Figure SI3 of the Supporting Information). The logarithmic plot (log(MSD) vs log(t)) reveals normal (Fickian) diffusion (slope $m \approx 1$), despite cation intercalation. This behavior stems from the interlayer spacing's capacity to accommodate three water layers, preventing steric crowding and maintaining bulk-like mobility. The absence of subdiffusive exponents ($m \approx 0.5$) excludes single-file or strongly confined diffusion under these conditions, consistent with expectations for such hydrated systems.

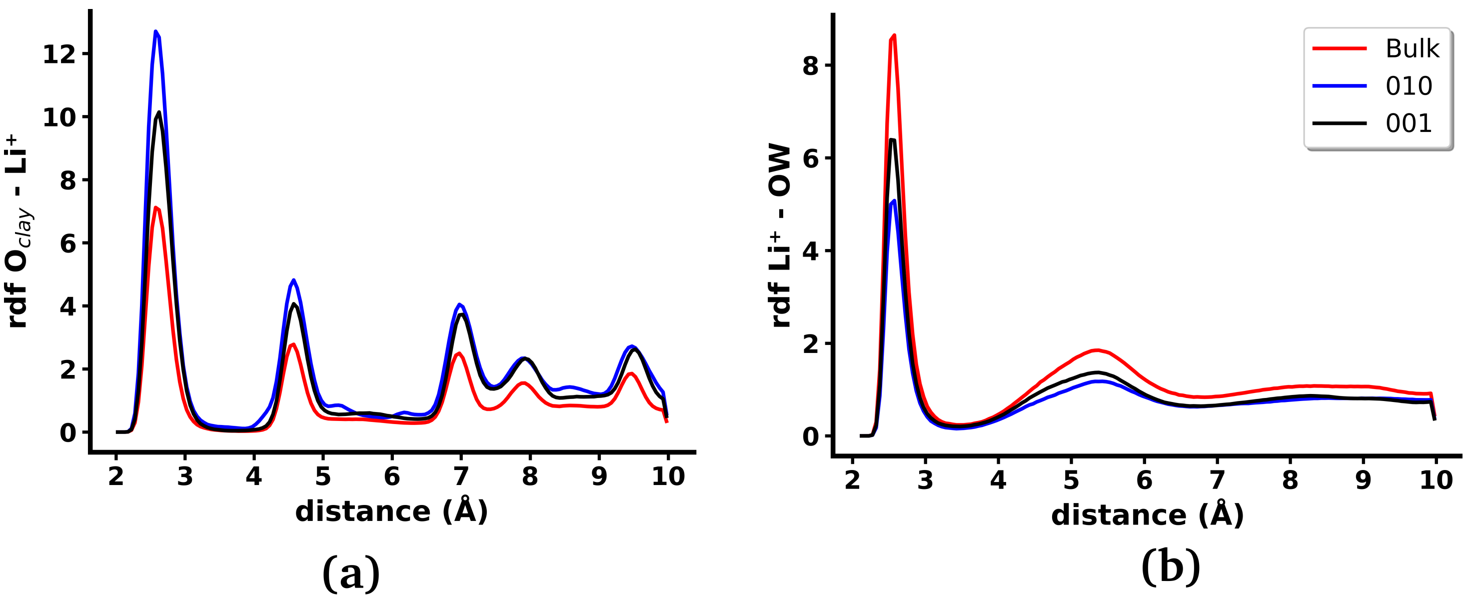

(a)

(b)

Figure 3. Radial distribution function (a) O_{clay}-Li^+ and (b) Li^+-OW for the three different models: bulk (red line), 010 (blue line) and 001 (black line).

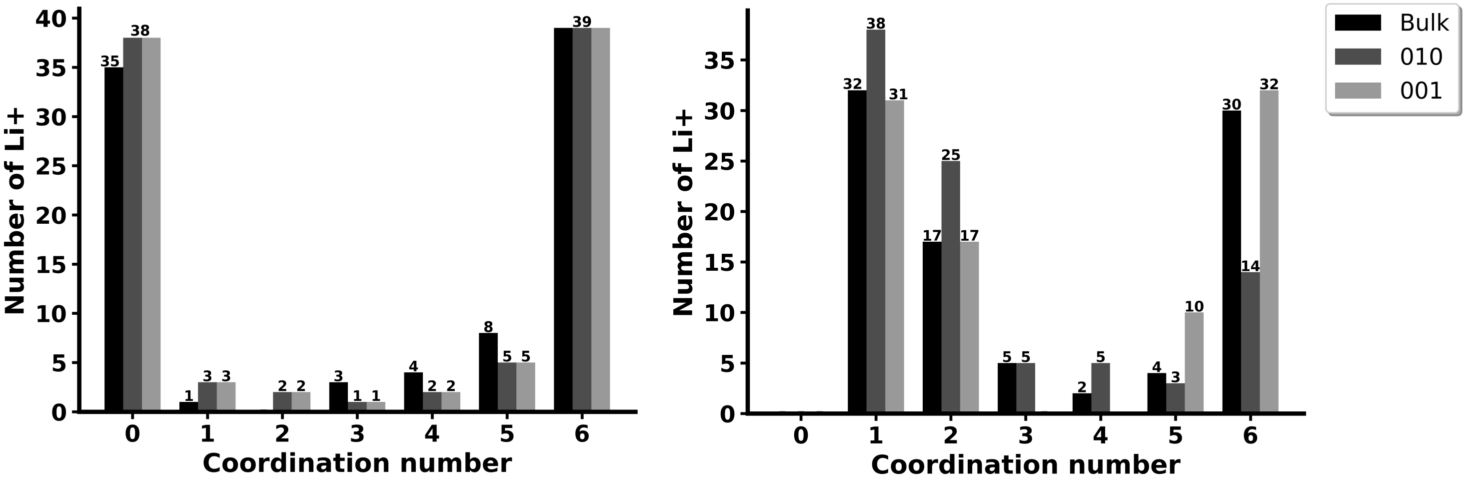

Figure 4. Number of Li^+ coordinated with (a) with clay oxygens (b) with water molecules.

Li^+ cations exhibit a jump diffusion mechanism characterized by rapid displacements. The same diffusion mechanism has been observed in our models with q = -2*e* [12]. Figure SI4 shows examples of displacements ($\mathbf{r}-\mathbf{r}_0$) as a function of time for selected Li^+, representative of movements II to V. Initially, Li^+ labeled 117 (green line in Fig. SI4) is located on a clay layer at the surface in contact with the water reservoir. This cation traverses the water reservoir during the simulation and is finally located on the opposite clay layer, having traveled a distance of 30 Å. In contrast, the labeled Li^+ 78 (black line in Fig. SI4) moves through the interlayer space. Between 9.2 ns and 14.825 ns it is confined in a hexagonal cage within the same layer. Then it diffuses back into the interlayer space, moving through it and approaching both layers. The trajectory of Li^+ 2028 (blue line in Fig. SI4) is also shown. Similar to cation 78, it diffuses through the interlayer space and approaches the opposite clay sheet for about 5.7 ns. It then remains in a hexagonal cage of the opposite sheet for about 3 ns before returning to the interlayer space. Later, at 10 ns and again at 16.5 ns, it returns to another hexagonal cage in the same layer where it was at 5.7 ns. Cations 78 and 2028 exhibit type II, III, and V motions.

The interaction of the lithium cations with clay and water significantly affects cation diffusion. This interaction can be evaluated using radial distribution functions (rdfs) and population analysis. Figure 3 shows the rdfs of lithium cations with oxygen from clay (O_{clay}-Li^+) and with oxygen from water (Li^+-OW) for the evaluated models. The rdfs for O_{clay}-Li^+ and Li^+-OW are very similar in all three models and closely resemble those obtained in the LiFh clay model with q = -2*e* [12]. The maximum of the first peaks, associated with the coordination of Li^+ with oxygens, in both O_{clay}-Li^+ and Li^+-OW is approximately 2.575.

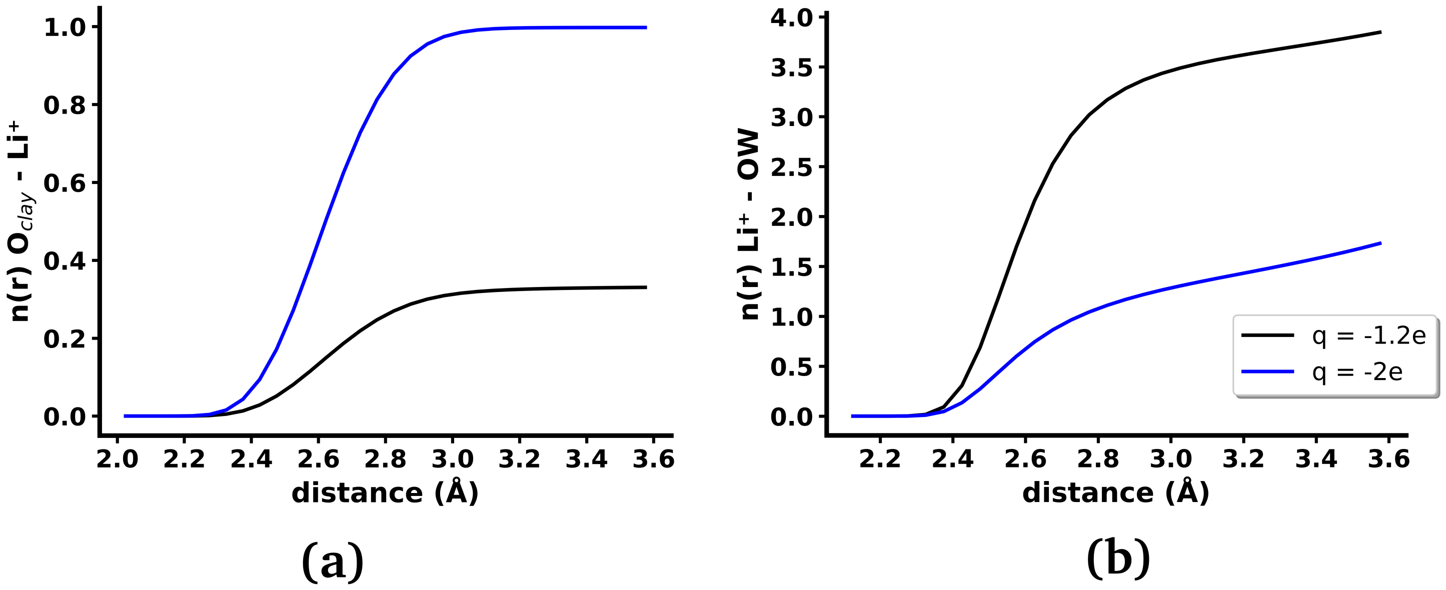

Figure 5. (a) n(r) O_{clay}-Li^+ and (b) n(r) Li^+-OW for the 001 model with charge equal -2*e* (blue line) and -1.2*e* (black line).

Figure 4 shows the coordination number of Li^+ cations with oxygen atoms from both clay and water molecules, calculated for Li^+-O distances shorter than 3 Å, using the final production run configuration for all three models. As observed, all Li^+ cations are coordinated with at least one water molecule. Those Li^+ cations that remain in their position or move to another hexagonal cage in their layer or in the opposite layer (movements I, II, and V, respectively) are coordinated with six oxygen atoms of the clay framework and with few water molecules. In contrast, Li^+ cations located in the interlayer space or diffusing into the bulk water (type III or IV motions) are expected to coordinate with a larger number of water molecules rather than the clay oxygens.

In the bulk and the 001 models, low (1) and high (6) coordination with clay and water molecules predominate, which is consistent with the results shown in Table 2. In these models, Li^+ cations are mainly located near the clay or in the interlayer space. Furthermore, there are more Li^+ cations coordinated with 5 or 6 water molecules in these models compared to the 010 model.

In the 010 model, there are more Li^+ cations coordinated with 1 and 2 water molecules. This difference is probably due to the deformation of the 010 model in the presence of water. Finally, the role of the clay charge on the mobility of the compensating cations can be better understood by analyzing the population functions, n(r), obtained from the radial distribution functions (rdf). In the Li-Fh models with a charge of -2*e* that we used previously [12], each oxygen atom in the clay experienced at least one Li^+ cation at a distance of less than 3 Å (blue line in Figure 5a). This is only possible when Li^+ is placed in the center of the hexagonal cage.

When the charge of the clay model is -1.2*e*, the value of n(r) decreases by 0.2, indicating that only 2 out of 10 oxygen atoms in the clay have a Li^+ cation at distances less than 3 Å. In contrast, the value of n(r) for Li^+-OW, which provides information about the average number of water molecules at distances lower than 3 for each Li^+ cation, increases from 1 to 3.5. This suggests that as the clay charge decreases, the cations interact less with the framework of the material and more with water molecules, leading to increased diffusion of Li^+ cations.

IV. CONCLUSION

Model 31 was found to be the most stable of the one hundred Li-Fh models generated with a charge of -1.2e. Based on this, three models were constructed: bulk, 010, and 001. The diffusion and movement of Li+ cations were studied in all three models. Li+ cations can move within the interlayer space, jump into hexagonal cavities within the same or opposite layers, and diffuse into the solution in the surface models. They can also migrate to other layers or to the edge of the octahedral sheet in the 010 model. In Li-Fh models with -1.2*e* charge, a larger number of Li+ ions diffuse with diffusion coefficients two orders of magnitude higher than in models with -2e charge. The diffusion coefficients (D) are similar in the three models, following the order 001 > 010 > Bulk. The compensating cations coordinate with a high number of clay oxygens (6) when they are in the hexagonal cavity of the clay lattice, or with a high number of water molecules (6) when they are in the interlayer or diffuse into the solution. The n(r) values also indicate that Li+ ions interact with a greater number of water molecules in the lower charge models. When the 010 model is in contact with a water reservoir, the osmotic swelling process occurs, leading to the observation of layer deformation resulting in a ”house of cards”structure. A significant number of Li+ cations are trapped in the deformed structure, which is why the value of D is lower in this model than in the 001 model. The results demonstrate the importance of the clay charge for understanding the movement of Li+

cations, their interaction with clay and water molecules, and the accurate reproducibility of delamination and swelling processes of clays.

V. SUPPORTING INFORMATION

The supplementary online materials include the Python code for generating nonhomogeneous LiFh models, the force fields model description, description of the thermal energy contribution in the clay-water system, and URL links to simulation videos.

VI. ACKNOWLEDGEMENTS

The authors would like to thank Cuban National Programs PN211LH008-027 and PN223LH010-017 for financial support.

REFERENCES

[1] F. Bergaya, B. K. G. Theng, G. Lagaly, *Handbook of Clay Science: Clay Mineral Control of Soil Organic Matter: A Conceptual Model Based on Physical Interactions* (Elsevier, 2006).
[2] M. Yu, S. M. Tariq, H. Yang, Clay Minerals **57**, 51 (2022).
[3] S. Khan, S. Ajmal, T. Hussain, M. U. Rahman, J. UQ. Univ. Appl. Sci. **9**, 1 (2023).
[4] Y. Lan, Y. Liu, J. Li, D. Chen, G. He, I. P. Parkin, Adv. Sci. **8**, 2004036 (2021).
[5] A. C. D. Newman, Phil. Trans. R. Soc. Lond. A **311**, 375 (1984).
[6] B. O. Otunola y O. O. Ololade, Environ. Tech. & Innov. **18**, 100692 (2020).
[7] A. Ochirkhuyag, J. Temuujin, Minerals **14**, 629 (2024).
[8] J. Dong, Z. Cheng, S. Tan, y Q. Zhu, Expert Opin. Drug Deliv. **18**, 695 (2020).
[9] C. Aguzzi, P. Cerezo, C. Viseras, C. Caramella, Appl. Clay Sci. **36**, 22 (2007).
[10] M. M. Orta, J. Martín, J. L. Santos, I. Aparicio, S. Medina-Carrasco, E. Alonso, Appl. Clay Sci. **198**, 105838 (2020).
[11] H. Kalo, M. W. Möller, D. A. Kunz, J. Breu, Nanoscale **4**, 5633 (2012).
[12] A. Lam y G. Rojas-Lorenzo, Rev. Cubana Fis. **41**, 10 (2024).
[13] R. P. Tenório, M. Engelsberg, J. O. Fossum, G. J. da Silva, Langmuir **26**, 9703 (2010).
[14] L. Michels, C. L. S. da Fonseca, Y. Méheust, M. A. S. Altoé, E. C. dos Santos, G. Grassi, R. Droppa Jr., K. D. Knudsen, L. P. Cavalcanti, K. W. B. Hunvik, J. O. Fossum, G. J. da Silva, H. N. Bordallo, J. Phys. Chem. C **124**, 24690 (2020).
[15] A. Lam, G. Rojas-Lorenzo, Rev. Cubana Fis. **39**, 85 (2022).
[16] R. T. Cygan, J. J. Liang, A. G. Kalinichev, J. Phys. Chem. B **108**, 1255 (2004).
[17] M. Pouvreau, J. A. Greathouse, R. T. Cygan, A. G. Kalinichev, J. Phys. Chem. C **123**, 11628 (2019).
[18] S. Koneshan, J. C. Rasaiah, R. M. Lynden-Bell, S. H. Lee, J. Phys. Chem. B **102**, 4193 (1998).
[19] I. Todorov, W. Smith, K. Trachenko, M. Dove, J. Mater. Chem. **16**, 1911 (2006).
[20] W. G. Hoover, Phys. Rev. A **31**, 1695 (1985).
[21] S. Nosé, J. Chem. Phys. **81**, 511 (1984).
[22] M. P. Allen, D. J. Tildesley, *Computer Simulation of Liquids*, 2nd ed. (Oxford University Press, Oxford, UK, 2017).
[23] P. E. Smith, B. M. Pettitt, Comput. Phys. Commun. **91**, 339 (1995).
[24] F. Kraehenbuehl, H. F. Stoeckli, F. Brunner, G. Kahr, M. Mueller-Vonmoos, Clay Minerals **1**, 1 (1987).
